# Bifurcation Analysis of a Non-linear On-Board Rotor-Bearing System

M. Zaki Dakel, Sébastien Baguet, Régis Dufour

# BIFURCATION ANALYSIS OF A NON-LINEAR ON-BOARD ROTOR-BEARING SYSTEM

**Mzaki Dakel**
Université de Lyon, CNRS,
INSA-Lyon, LaMCoS UMR5259,
F-69621, France
mzaki.dakel@insa-lyon.fr

**Sébastien Baguet**
Université de Lyon, CNRS,
INSA-Lyon, LaMCoS UMR5259,
F-69621, France
sebastien.baguet@insa-lyon.fr

**Régis Dufour**
Université de Lyon, CNRS,
INSA-Lyon, LaMCoS UMR5259,
F-69621, France
regis.dufour@insa-lyon.fr

## ABSTRACT

*The non-linear dynamic behavior of an on-board rotor mounted on hydrodynamic journal bearings and subject to rigid base excitations is investigated in this work. The proposed finite element rotor model takes into account the geometric asymmetry of shaft and/or rigid disk and considers six types of base deterministic motions (rotations and translations) and non-linear fluid film forces obtained from the Reynolds equation. The equations of motion contain time-varying parametric coefficients because of the geometric asymmetry of the rotor and the base rotations. In the case when sinusoidal excitations of the rotor base lead to periodic (harmonic and sub-harmonic) responses, an optimized shooting algorithm based on the non-linear Newmark time integration scheme is employed to solve the equations of motion. The non-linear phenomena observed in the on-board rotor-bearing system, such as period-doubling motion and chaos, are characterized by means of bifurcation diagrams, rotor orbits and Poincaré maps.*

## 1 INTRODUCTION

The rotating machines occupy an important position in our life and play a paramount role in the modern industry. The rotor represents their key component and is subject to base excitations when it is embedded in moving systems. Vehicle turbochargers and gas turbine rotors installed in power plants are especially concerned with such a situation.

The rotor systems are complex and their dynamic analysis is rather difficult. Several studies focused on making a clear understanding of the dynamics of symmetric/asymmetric rigid/flexible rotor systems supported by linear/non-linear elastic bearings in the case of a fixed base, see, for example, Lalanne and Ferraris [1] and Genta [2]. Berlioz et al. [3] investigated numerically and experimentally the bifurcation of solutions of the non-linear equations of motion with periodic parameters for an on-board pendulum. Oncescu et al. [4] generalized a finite element procedure for rotor-bearing systems to include the effects of the asymmetry of shaft and/or bearing and predicted the dynamic behavior of such systems.

The rotor-hydrodynamic bearing system is fully non-linear due to non-linear fluid forces acting locally on it. Li and Xu [5] studied a Jeffcott rotor mounted on fluid film infinite-length bearings to predict periodic orbits, their periods and their stability by employing the generalized shooting method. Bifurcation diagrams as well as harmonic, sub-harmonic and quasi periodic responses and their Poincaré maps were investigated for a flexible rotor (Chen and Yau [6]) and a vertical rigid rotor (Shi et al. [7]) supported by hydrodynamic short bearings.

Srinivasan and Soni [8] examined the influence of spin, base rotation as well as axial force and axial torque on the seismic response of a rotor-bearing system. Hori and Kato [9] studied the seismic response of a Jeffcott rotor supported by fluid film bearings to a real seismic wave and investigated its stability by calculating the locations of the disk and journal centers. Kang et al. [10] and Cavalca et al. [11] observed the influence of the flexible supporting structure on the dynamic characteristics of the rotor-bearing systems.

The number of works dealing with the prediction of dynamic behavior of the rotor systems excited by a sinusoidal motion of their base remains actually low. Duchemin et al. [12] employed the method of multiple scales for a simple rotor model under a sinusoidal rotation of the base in order to observe its dynamic stability. They showed also experimental results to validate the analytical study. Driot et al. [13] presented numerical orbits of a rotor induced by a sinusoidal rotational excitation of its base. According to their work, the comparison between numerical and experimental results was widely satisfactory. El-Saeidy and Sticher [14] calculated the responses of a rigid rotor-bearing system subject to rotating mass unbalance and sinusoidal movements of the base along or

around lateral directions using analytical solutions in the case of linear bearings and a time integration scheme in the case of a bearing cubic non-linearity. Das et al. [15] executed a numerical simulation of a flexible rotor system excited by a mass unbalance and a sinusoidal rotation of the base in order to investigate its active vibration control which was successful for avoiding the lateral parametric instability. Dakel et al. [16] computed the orbits and their spectral analysis for a rotor mounted on linearized hydrodynamic short bearings and excited by combined rotational and translational motions of its base. They predicted also the linear dynamic behavior of symmetric and asymmetric rotors on rigid bearings subject to combined constant rotation and sinusoidal translation of the base [17]. More recently, they presented a comparison between linear and non-linear responses of a rotor mounted on hydrodynamic short bearings and excited by sinusoidal motions of the base to assess the validity range of the linearized bearing model [18].

The present work is mainly based on the model presented in [18] but investigates in more detail the non-linear effects due to the combination of a non-linear rotor-bearing system (because of fluid film forces) and base excitations. The proposed on-board rotor is discretized using the finite element method based on the Timoshenko beam theory and excited by combined deterministic motions (three rotations and three translations) of its rigid base. The rotary inertia, the gyroscopic inertia, the shear deformation of shaft as well as the geometric asymmetry of shaft and/or rigid disk are taken into account. The non-linear hydrodynamic fluid forces within the bearing are evaluated by the Reynolds equation and treated as restoring forces acting on the shaft. The application of the Lagrange's equations gives the non-linear differential equations of motion of the rotor in bending with respect to a non-inertial reference frame linked with the rigid base. These equations point out periodic parametric terms due to the geometric asymmetry of the rotor and time-varying parametric terms due to the rotational excitations of the base. The transient implicit Newmark time-step integration scheme combined with the Newton-Raphson iterative strategy is employed to treat the equations of motion. In addition, in the case when sinusoidal motions of the rotor base yield periodic (harmonic and sub-harmonic) responses, an optimized shooting method is used to treat the equations of motion. The non-linear phenomena identified in the on-board rotor are described by means of bifurcation diagrams, rotor orbits as well as Poincaré maps.

## 2 PRELIMINARY CALCULATIONS

The rotor frequently consists of the disk, shaft, mass unbalance, bearing and base. The excitations taken into account are due to the mass unbalance and to the rigid base motions. Three principal Cartesian coordinate systems shown in Fig. 1 are introduced to take into consideration the mobility of the rotor base. They are attached to the ground $R^g$, the rigid base $R$ and the moving rotor $R^l$.

The translational motions of the rotor base are defined by the coordinates $x_O(t)$, $y_O(t)$ and $z_O(t)$ of the position vector $\mathbf{O^gO}$ of the origin $O$ expressed in the frame fixed to the base $R$. The rotational motions of the rotor base are defined by the angular velocity vector components $\omega^x(t)$, $\omega^y(t)$ and $\omega^z(t)$ of the rigid base $R$ with respect to the ground $R^g$ projected in the frame $R$.

A generic point $C^{init}$ on the elastic line of the non-deformed shaft is considered. Its coordinates in the frame $R$ are $(0,y,0)$. Its lateral dynamic displacements $u(y,t)$ and $w(y,t)$ due to bending are expressed respectively with respect to the $Ox$ and $Oz$ axes. Additional details on the kinematics of the on-board rotor can be found in [17,18].

## 3 ENERGY AND VIRTUAL WORK CALCULATIONS

**Disk, Shaft and Mass Unbalance.** The necessary equations have been established in [17,18] and the calculations are briefly described hereafter.

Since the disk is assumed to be rigid, only its kinetic energy is computed. The kinetic energy of a shaft elementary volume is considered as a generalization of the case of a disk. Moreover, the strain energy of the shaft is calculated using the Timoshenko beam theory. The mass unbalance located on the disk is characterized by its kinetic energy.

**Hydrodynamic Journal Bearing.** The short bearing theory is considered in this study. At a constant speed of rotation $\Omega$ of the rotor and for a constant static load $W_r$ created by the rotor weight, the shaft geometric center ${C_{be}}^0$ in the bearing holds a static equilibrium position defined by the displacement vector $\boldsymbol{\delta}_{be}{}^0=\langle u_{be}{}^0, w_{be}{}^0\rangle_R{}^T$ expressed in $R$.

In the dynamic regime, the dynamic transverse displacement vector of the shaft center is $\boldsymbol{\delta}_{be}=\langle u_{be}, w_{be}\rangle_R{}^T$. Assuming an isothermal and laminar flow of an isoviscous incompressible fluid, the hydrodynamic fluid pressure field is analytically calculated with the Reynolds equation. Its integration using the Gümbel boundary conditions leads to the dynamic polar (tangential and radial) components of the hydrodynamic force vector expressed in the polar frame linked with the hydrodynamic bearing $R^{be}$ and defined by the following formulations (see [19])

$$F_{be}^{ta} = \frac{\mu_{be} r_{be} l_{be}^3 \varepsilon_{be}}{2c_{be}^2\left(1-\varepsilon_{be}^2\right)^2}\left(4\dot{\varepsilon}_{be} + \frac{\pi}{2}\sqrt{1-\varepsilon_{be}^2}\left(\Omega - 2\dot{\varphi}_{be}\right)\right),$$
$$F_{be}^{ra} = -\frac{\mu_{be} r_{be} l_{be}^3}{2c_{be}^2\left(1-\varepsilon_{be}^2\right)^2}\left(\frac{\pi\dot{\varepsilon}_{be}\left(1+2\varepsilon_{be}^2\right)}{\sqrt{1-\varepsilon_{be}^2}} + 2\varepsilon_{be}^2\left(\Omega - 2\dot{\varphi}_{be}\right)\right), \quad (1)$$

with

$$\varepsilon_{be} = \frac{\sqrt{u_{be}^2 + w_{be}^2}}{c_{be}} \quad ; \quad \tan\varphi_{be} = \frac{u_{be}}{w_{be}}, \quad (2)$$

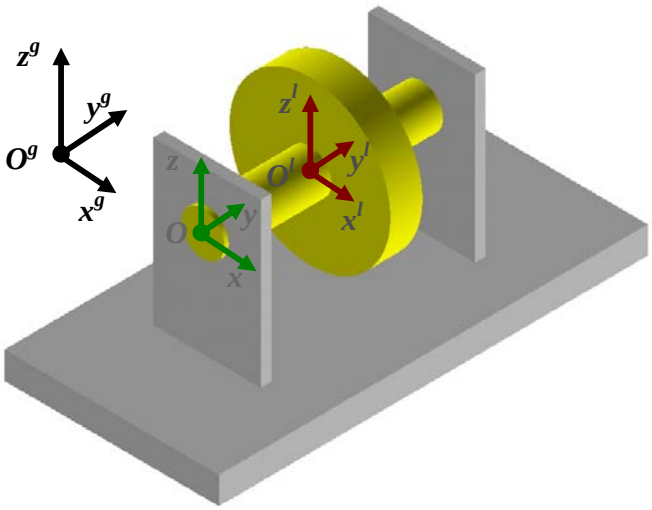


**Figure 1. FRAMES OF REFERENCE FOR THE ON-BOARD ROTOR**

$$\dot{\varepsilon}_{be} = \frac{\dot{u}_{be}u_{be} + \dot{w}_{be}w_{be}}{c_{be}^2\varepsilon_{be}} \quad ; \quad \dot{\varphi}_{be} = \frac{\dot{u}_{be}w_{be} - \dot{w}_{be}u_{be}}{c_{be}^2\varepsilon_{be}^2}, \tag{3}$$

where $\mu_{be}$, $r_{be}$, $l_{be}$ and $c_{be}$ are respectively the dynamic viscosity, radius, length, clearance of the bearing. $\varepsilon_{be}$ and $\varphi_{be}$ are the relative dynamic eccentricity and the dynamic attitude angle.

The components of the dynamic fluid force vector $\mathbf{F}_{be}=<F_{be}{}^{u},F_{be}{}^{w}>_R{}^T$ projected in the frame $R$ are obtained by a classical change of basis between the frames $R^{be}$ and $R$. They are non-linear functions of the dynamic transverse displacement and velocity vectors $\left(\boldsymbol{\delta}_{be},\dot{\boldsymbol{\delta}}_{be}\right)$. Since the bearing contribution appears as forces $\mathbf{F}_{be}$ external to the rotor, their virtual work $\delta W_{be}$ has to be established to apply the Lagrange's equations

$$\delta W_{be} = \mathbf{F}_{be}^T\left(\boldsymbol{\delta}_{be},\dot{\boldsymbol{\delta}}_{be}\right)\delta\boldsymbol{\delta}_{be}. \tag{4}$$

## 4 EQUATIONS OF MOTION

The finite element method is selected to discretize the rotor and to describe its flexural motion as a function of the nodal displacement vector defined by $\boldsymbol{\delta}^n=<u^n,w^n,\theta^n,\psi^n>_R{}^T$, i.e., the rotor has two lateral translations and two rotations at each node. The shaft finite element has two nodes and the shape functions are based on the Timoshenko beam theory.

The non-linear equations of motion of the on-board rotor-bearing system in bending are obtained after applying the Lagrange's equations to the energies for the disk, the shaft finite elements and the mass unbalance as well as to the virtual work of the hydrodynamic bearings and assembling appropriately the produced vectors and matrices. They are written with respect to the non-inertial frame connected to the base $R$ as follows

$$\mathbf{M}(t)\ddot{\boldsymbol{\delta}} + \mathbf{C}(t)\dot{\boldsymbol{\delta}} + \mathbf{K}(t)\boldsymbol{\delta} = \mathbf{F}(t) + \mathbf{F}_{be}\left(\boldsymbol{\delta},\dot{\boldsymbol{\delta}}\right), \tag{5}$$

with $\ddot{\boldsymbol{\delta}}$, $\dot{\boldsymbol{\delta}}$ and $\boldsymbol{\delta}$ the acceleration, velocity and displacement vectors of the on-board rotor-bearing system of dimension $4(n_{esh}+1)\times 1$ where $n_{esh}$ is the number of shaft finite elements. $\mathbf{M}(t)$, $\mathbf{C}(t)$ and $\mathbf{K}(t)$ are respectively the mass, damping and stiffness matrices with time-varying coefficients due to the asymmetry of the rotating rotor and to its moving base. $\mathbf{F}(t)$ is the external linear force vector due to the mass unbalance and to the rotational and translational motions of the base. In addition, the external non-linear hydrodynamic force vector $\mathbf{F}_{be}\left(\boldsymbol{\delta},\dot{\boldsymbol{\delta}}\right)$ of the bearings is opposite to the rotor motion.

The matrices of Eq. (5) are defined as follows

$$\mathbf{M}(t) = \mathbf{M}_{d,sh} + \mathbf{M}_{d,sh}^{c_2}\cos 2\Omega t + \mathbf{M}_{d,sh}^{s_2}\sin 2\Omega t, \tag{6}$$

$$\mathbf{C}(t) = \mathbf{C}_{d,sh}^{g}\Omega + \mathbf{C}_{d,sh}^{g,c_2}\Omega\cos 2\Omega t + \mathbf{C}_{d,sh}^{g,s_2}\Omega\sin 2\Omega t + \mathbf{C}_{d,sh,b}^{re,\omega^y}\omega^y, \tag{7}$$

$$\begin{aligned}\mathbf{K}(t) = {} & \mathbf{K}_{sh}^{e} + \mathbf{K}_{sh}^{e,c_2}\cos 2\Omega t + \mathbf{K}_{sh}^{e,s_2}\sin 2\Omega t \\ & + \mathbf{K}_{d,sh,b}^{re,\dot{\omega}^y}\dot{\omega}^y + \mathbf{K}_{d,sh,b}^{re,\Omega\omega^y}\Omega\omega^y + \left(\mathbf{K}_{d,sh,b}^{re,\omega^{x2}} + \mathbf{K}_{d,sh,b}^{gse,\omega^{x2}}\right)\omega^{x2} \\ & + \mathbf{K}_{d,sh,b}^{re,\omega^{y2}}\omega^{y2} + \left(\mathbf{K}_{d,sh,b}^{re,\omega^{z2}} + \mathbf{K}_{d,sh,b}^{gse,\omega^{z2}}\right)\omega^{z2} + \mathbf{K}_{d,sh,b}^{re,\omega^x\omega^z}\omega^x\omega^z \\ & + \left(\mathbf{K}_{d,sh,b}^{re,\dot{\omega}^y,c_2}\dot{\omega}^y + \mathbf{K}_{d,sh,b}^{re,\Omega\omega^y,c_2}\Omega\omega^y + \mathbf{K}_{d,sh,b}^{re,\omega^{x2},c_2}\omega^{x2}\right. \\ & \left. + \mathbf{K}_{d,sh,b}^{re,\omega^{y2},c_2}\omega^{y2} + \mathbf{K}_{d,sh,b}^{re,\omega^{z2},c_2}\omega^{z2} + \mathbf{K}_{d,sh,b}^{re,\omega^x\omega^z,c_2}\omega^x\omega^z\right)\cos 2\Omega t \\ & + \left(\mathbf{K}_{d,sh,b}^{re,\dot{\omega}^y,s_2}\dot{\omega}^y + \mathbf{K}_{d,sh,b}^{re,\Omega\omega^y,s_2}\Omega\omega^y + \mathbf{K}_{d,sh,b}^{re,\omega^{x2},s_2}\omega^{x2}\right. \\ & \left. + \mathbf{K}_{d,sh,b}^{re,\omega^{y2},s_2}\omega^{y2} + \mathbf{K}_{d,sh,b}^{re,\omega^x\omega^z,s_2}\omega^x\omega^z\right)\sin 2\Omega t.\end{aligned} \tag{8}$$

The subscripts "*d*", "*sh*" and "*b*" refer to the disk, shaft as well as base respectively and express the contribution to the phenomenon represented by the corresponding matrix. The superscripts "$c_2$" and "$s_2$" signify the geometric asymmetry of the rotor expressed in terms of the time-varying trigonometric functions $\cos 2\Omega t$ and $\sin 2\Omega t$. The superscript "*g*" stands for the rotor gyroscopic effect, "*e*" for the shaft elasticity corresponding to the bending and shear deformations, "*re*" for the rotational effects corresponding to the rotational motions of the base (these effects come from the kinetic energies of the disk and the shaft) and "*gse*" for the geometric stiffening effects associated with the centrifugal stress due to the rotational motions of the base.

The vector $\mathbf{F}(t)$ is expressed as follows

$$\mathbf{F}(t) = \mathbf{F}_{d,sh}^{W_r} + \mathbf{F}_{mu}(t) + \mathbf{F}_{mu,b}(t) + \mathbf{F}_{d,sh,b}(t) + \mathbf{F}_{d,sh,b}^{c_2}(t)\cos 2\Omega t + \mathbf{F}_{d,sh,b}^{s_2}(t)\sin 2\Omega t, \tag{9}$$

with

$$\mathbf{F}_{d,sh}^{W_r} = -\mathbf{V}_{d,sh}^{W_r}W_r, \tag{10}$$

$$\mathbf{F}_{mu}(t) = \mathbf{V}_{mu}^{c_1}\Omega^2\cos\Omega t + \mathbf{V}_{mu}^{s_1}\Omega^2\sin\Omega t, \tag{11}$$

$$\begin{aligned}\mathbf{F}_{mu,b}(t) = &\left(\mathbf{V}_{mu,b}^{\dot{\omega}^y,c_1}\dot{\omega}^y + \mathbf{V}_{mu,b}^{\Omega\omega^y,c_1}\Omega\omega^y + \mathbf{V}_{mu,b}^{\omega^{x2},c_1}\omega^{x2} + \mathbf{V}_{mu,b}^{\omega^{y2},c_1}\omega^{y2}\right.\\ &\left.+\mathbf{V}_{mu,b}^{\omega^{z2},c_1}\omega^{z2} + \mathbf{V}_{mu,b}^{\omega^x\omega^z,c_1}\omega^x\omega^z\right)\cos\Omega t\\ &+\left(\mathbf{V}_{mu,b}^{\dot{\omega}^y,s_1}\dot{\omega}^y + \mathbf{V}_{mu,b}^{\Omega\omega^y,s_1}\Omega\omega^y + \mathbf{V}_{mu,b}^{\omega^{x2},s_1}\omega^{x2}\right.\\ &\left.+\mathbf{V}_{mu,b}^{\omega^{y2},s_1}\omega^{y2} + \mathbf{V}_{mu,b}^{\omega^{z2},s_1}\omega^{z2} + \mathbf{V}_{mu,b}^{\omega^x\omega^z,s_1}\omega^x\omega^z\right)\sin\Omega t,\end{aligned} \tag{12}$$

$$\begin{aligned}\mathbf{F}_{d,sh,b}(t) = &-\mathbf{V}_{d,sh,b}^{u}\left(\ddot{x}_O + 2\dot{z}_O\omega^y - 2\dot{y}_O\omega^z + z_O\left(\dot{\omega}^y + \omega^x\omega^z\right)\right.\\ &\left.-y_O\left(\dot{\omega}^z - \omega^x\omega^y\right) - x_O\left(\omega^{y2} + \omega^{z2}\right)\right)\\ &-\mathbf{V}_{d,sh,b}^{w}\left(\ddot{z}_O + 2\dot{y}_O\omega^x - 2\dot{x}_O\omega^y + y_O\left(\dot{\omega}^x + \omega^y\omega^z\right)\right.\\ &\left.-x_O\left(\dot{\omega}^y - \omega^x\omega^z\right) - z_O\left(\omega^{x2} + \omega^{y2}\right)\right)\\ &-\mathbf{V}_{d,sh,b}^{yw}\left(\dot{\omega}^x + \omega^y\omega^z\right) + \mathbf{V}_{d,sh,b}^{yu}\left(\dot{\omega}^z - \omega^x\omega^y\right)\\ &-\mathbf{V}_{d,sh,b}^{\theta}\left(\dot{\omega}^x + \omega^y\omega^z\right) - \mathbf{V}_{d,sh,b}^{\psi}\left(\dot{\omega}^z - \omega^x\omega^y\right)\\ &-\mathbf{V}_{d,sh,b}^{y\psi}\left(\Omega\omega^x + \omega^x\omega^y\right) + \mathbf{V}_{d,sh,b}^{y\theta}\left(\Omega\omega^z + \omega^y\omega^z\right),\end{aligned} \tag{13}$$

$$\begin{aligned}\mathbf{F}_{d,sh,b}^{c_2}(t) = &-\mathbf{V}_{d,sh,b}^{\theta,c_2}\left(\dot{\omega}^x - 2\Omega\omega^z - \omega^y\omega^z\right)\\ &+\mathbf{V}_{d,sh,b}^{\psi,c_2}\left(\dot{\omega}^z + 2\Omega\omega^x + \omega^x\omega^y\right),\end{aligned} \tag{14}$$

$$\begin{aligned}\mathbf{F}_{d,sh,b}^{s_2}(t) = &\mathbf{V}_{d,sh,b}^{\psi,s_2}\left(\dot{\omega}^x - 2\Omega\omega^z - \omega^y\omega^z\right)\\ &+\mathbf{V}_{d,sh,b}^{\theta,s_2}\left(\dot{\omega}^z + 2\Omega\omega^x + \omega^x\omega^y\right),\end{aligned} \tag{15}$$

where $\mathbf{V}_{mu}$ ($\mathbf{F}_{mu}(t)$), $\mathbf{V}_{d,sh,b}$ ($\mathbf{F}_{d,sh,b}(t)$) and $\mathbf{V}_{mu,b}$ ($\mathbf{F}_{mu,b}(t)$) are load vectors (force vectors) associated respectively with the mass unbalance, the inertia force due to base motions and that due to coupling between both phenomena. $\mathbf{F}_{d,sh}^{W_r}$ is the rotor weight vector. The superscripts "$c_1$" and "$s_1$" denote the components of the mass unbalance force expressed in terms of the time-varying trigonometric functions cos$\Omega t$ and sin$\Omega t$. The superscripts $u$, $w$, $\psi$ and $\theta$ denote the direction of the action force components associated with the motions of the rotor base.

As already stated above, the equations of motion are non-linear. This is due to the hydrodynamic bearings (local components) even if they do not concern all the degrees of freedom of the rotor system. In the two following sections (i.e., Sections 5 and 6), the treatment of these equations is detailed.

## 5 TRANSIENT DYNAMIC ANALYSIS

The resolution of the complete non-linear dynamic problem requires solving simultaneously the equations of motion (i.e., Eq. (5)) of the rotor-bearing system and Eqs. (1)-(3) calculating the non-linear hydrodynamic bearing forces governed by the Reynolds equation in the dynamic regime. Therefore the non-linear analysis uses a complex procedure combining the Newton-Raphson incremental-iterative technique with the Newmark time integration algorithm. The semi-discrete equations of motion (Eq. (5)) applied at time $t_{i+1}$ ($1 \le i \le n_{ts}+1$ where $n_{ts}$ is the number of time steps) can be given in the following residual form

$$\begin{aligned}\mathbf{G}(\boldsymbol{\delta}_{i+1}) = &\mathbf{M}(t_{i+1})\ddot{\boldsymbol{\delta}}_{i+1} + \mathbf{C}(t_{i+1})\dot{\boldsymbol{\delta}}_{i+1} + \mathbf{K}(t_{i+1})\boldsymbol{\delta}_{i+1}\\ &-\mathbf{F}(t_{i+1}) - \mathbf{F}_{be}\left(\boldsymbol{\delta}_{i+1}, \dot{\boldsymbol{\delta}}_{i+1}\right) = \mathbf{0}.\end{aligned} \tag{16}$$

The velocity and displacement vectors of the rotor nodes between $t_i$ and $t_{i+1}=t_i+\Delta t$, $\Delta t$ being the time step, are approximated by the following general formulations of the implicit Newmark scheme

$$\begin{aligned}\dot{\boldsymbol{\delta}}_{i+1} &= \dot{\boldsymbol{\delta}}_i + \Delta t\left(\alpha\ddot{\boldsymbol{\delta}}_{i+1} + (1-\alpha)\ddot{\boldsymbol{\delta}}_i\right),\\ \boldsymbol{\delta}_{i+1} &= \boldsymbol{\delta}_i + \Delta t\dot{\boldsymbol{\delta}}_i + \frac{(\Delta t)^2}{2}\left(2\beta\ddot{\boldsymbol{\delta}}_{i+1} + (1-2\beta)\ddot{\boldsymbol{\delta}}_i\right),\end{aligned} \tag{17}$$

where the parameters $\alpha$=1/2 and $\beta$=1/4 define the constant average acceleration scheme. As Eq. (16) is non-linear, an iterative procedure is employed to treat the non-linearity. Namely, the linearization of Eq. (16) is performed by building a first-order Taylor series of this equation and the Newton-Raphson iterative strategy is taken into consideration as follows

$$\mathbf{G}\left(\boldsymbol{\delta}_{i+1}^{k+1}\right) \simeq \mathbf{G}\left(\boldsymbol{\delta}_{i+1}^{k}\right) + \left.\frac{d\mathbf{G}}{d\boldsymbol{\delta}_{i+1}}\right|_{\left(\boldsymbol{\delta}_{i+1}^{k}\right)} \Delta\boldsymbol{\delta} = \mathbf{0}, \tag{18}$$

then

$$\mathbf{J}^{NL}\left(\boldsymbol{\delta}_{i+1}^{k}\right)\Delta\boldsymbol{\delta} = -\mathbf{G}\left(\boldsymbol{\delta}_{i+1}^{k}\right), \tag{19}$$

where $\Delta\boldsymbol{\delta} = \boldsymbol{\delta}_{i+1}^{k+1} - \boldsymbol{\delta}_{i+1}^{k}$ is the iterative increment of the displacement vector and $k$ is the Newton-Raphson iteration. The Jacobian matrix $\mathbf{J}^{NL}$ is a function of the displacement vector $\boldsymbol{\delta}_{i+1}$ at iteration $k$ and expressed by

$$\begin{aligned}\mathbf{J}^{NL}\left(\boldsymbol{\delta}_{i+1}^{k}\right) = \left.\frac{d\mathbf{G}}{d\boldsymbol{\delta}_{i+1}}\right|_{\left(\boldsymbol{\delta}_{i+1}^{k}\right)} &= \frac{1}{\beta(\Delta t)^2}\mathbf{M}(t_{i+1}) + \frac{\alpha}{\beta\Delta t}\mathbf{C}(t_{i+1})\\ &+\mathbf{K}(t_{i+1}) - \left.\frac{d\mathbf{F}_{be}}{d\boldsymbol{\delta}_{i+1}}\right|_{\left(\boldsymbol{\delta}_{i+1}^{k}, \dot{\boldsymbol{\delta}}_{i+1}^{k}\right)},\end{aligned} \tag{20}$$

where $\mathbf{I}$ is the identity matrix. The derivative of the non-linear hydrodynamic forces in the Jacobian matrix of Eq. (20) is a function of both the displacement and velocity vectors $\left(\boldsymbol{\delta}_{i+1}^{k}, \dot{\boldsymbol{\delta}}_{i+1}^{k}\right)$, updated at each iteration $k$ and expressed by

$$\left.\frac{d\mathbf{F}_{be}}{d\boldsymbol{\delta}_{i+1}}\right|_{\left(\boldsymbol{\delta}_{i+1}^{k}, \dot{\boldsymbol{\delta}}_{i+1}^{k}\right)} = \left.\frac{\partial\mathbf{F}_{be}}{\partial\boldsymbol{\delta}_{i+1}}\right|_{\left(\boldsymbol{\delta}_{i+1}^{k}, \dot{\boldsymbol{\delta}}_{i+1}^{k}\right)} + \frac{\alpha}{\beta\Delta t}\left.\frac{\partial\mathbf{F}_{be}}{\partial\dot{\boldsymbol{\delta}}_{i+1}}\right|_{\left(\boldsymbol{\delta}_{i+1}^{k}, \dot{\boldsymbol{\delta}}_{i+1}^{k}\right)}. \tag{21}$$

The procedure of the Newton-Raphson incremental-iterative strategy combined with the Newmark time integration scheme is presented as pseudo-code hereafter.

(1) Initial conditions $\boldsymbol{\delta}_1$ ; $\dot{\boldsymbol{\delta}}_1$

$$\ddot{\boldsymbol{\delta}}_1 = \mathbf{M}^{-1}(0)\left(\mathbf{F}(0) + \mathbf{F}_{\mathbf{be}}\left(\boldsymbol{\delta}_1, \dot{\boldsymbol{\delta}}_1\right) - \mathbf{C}(0)\dot{\boldsymbol{\delta}}_1 - \mathbf{K}(0)\boldsymbol{\delta}_1\right)$$

(2) Prediction step:

$$\ddot{\boldsymbol{\delta}}_{i+1}^1 = \ddot{\boldsymbol{\delta}}_i \; ; \; \dot{\boldsymbol{\delta}}_{i+1}^1 = \dot{\boldsymbol{\delta}}_i + \Delta t\ddot{\boldsymbol{\delta}}_i \; ; \; \boldsymbol{\delta}_{i+1}^1 = \boldsymbol{\delta}_i + \Delta t\dot{\boldsymbol{\delta}}_i + \frac{\Delta t^2}{2}\ddot{\boldsymbol{\delta}}_i$$

(3) Calculation of the hydrodynamic forces $\mathbf{F}_{be}\left(\boldsymbol{\delta}, \dot{\boldsymbol{\delta}}\right)$

(4) Residual calculation **G** with Eq. (16)

(5) Calculation of the Jacobian matrix $\mathbf{J}^{NL}$ with Eq. (20)

(6) Correction increment $\Delta\boldsymbol{\delta}$ with Eq. (19)

(7) Correction step:

$$\boldsymbol{\delta}_{i+1}^{k+1} = \boldsymbol{\delta}_{i+1}^{k} + \Delta\boldsymbol{\delta} \; ; \; \dot{\boldsymbol{\delta}}_{i+1}^{k+1} = \dot{\boldsymbol{\delta}}_{i+1}^{k} + \frac{\alpha}{\beta\Delta t}\Delta\boldsymbol{\delta},$$

$$\ddot{\boldsymbol{\delta}}_{i+1}^{k+1} = \ddot{\boldsymbol{\delta}}_{i+1}^{k} + \frac{1}{\beta(\Delta t)^2}\Delta\boldsymbol{\delta}$$

(8) Return to (3) for new hydrodynamic forces $\mathbf{F}_{be}\left(\boldsymbol{\delta}, \dot{\boldsymbol{\delta}}\right)$

(9) Return to (4) for a new residual **G**

(10) If $\|\mathbf{G}\|/\|\mathbf{F}\| > \varepsilon^{NL}$, return to (5) for a new Newton-Raphson iteration, else return to (2) for a new time step

In order to reach the steady-state periodic regime, the Newmark algorithm has to be used over a large number of time periods. This results in an enormous computational time when the algorithm is repeated for a large number of fundamental excitation frequencies. Computational time can be saved by seeking directly the periodic solution by means of the shooting method being discussed in the next section.

## 6 PERIODIC SOLUTION USING THE SHOOTING METHOD

The following two-point boundary-value problem defined by the periodicity condition is considered

$$\mathbf{H}\left(\mathbf{X}(0), t = \tau_r\right) = \mathbf{X}\left(\mathbf{X}(0), t = \tau_r\right) - \mathbf{X}(0) = \mathbf{0}, \tag{22}$$

with

$$\mathbf{X} = \left\langle \boldsymbol{\delta}^T, \dot{\boldsymbol{\delta}}^T \right\rangle^T, \tag{23}$$

where $\tau_r$ is the minimal period of the rotor response. The dependence of the system on the fundamental period $\tau_{ex}$ of the periodic exciting forces is assumed, i.e., $\tau_r = j\tau_{ex}$ (with $j$=1,2,3...). Integer multiples of the fundamental period are used to calculate sub-harmonic responses occurring, for example, after a period-doubling bifurcation. Practically, in order to find the minimal period $\tau_r$ of the response, the shooting method is first performed with $\tau_r = \tau_{ex}$ and if there is no convergence, it is then performed with $\tau_r = 2\tau_{ex}$, $\tau_r = 3\tau_{ex}$, ... successively. The state-space vector **X** in Eq. (22) is the solution of Eq. (5) at the end of one period $\tau_r$ for an approached initial solution **X**(0). This vector is computed by the non-linear Newmark time integration procedure over one period $\tau_r$ (see Section 5). A consistent linearization of Eq. (22) is made by finding a first-order Taylor series expansion of this equation and a Newton-Raphson iterative correction is executed

$$\mathbf{H}\left(\mathbf{X}^{k+1}(0), \tau_r\right) \simeq \mathbf{H}\left(\mathbf{X}^{k}(0), \tau_r\right) + \left.\frac{\partial \mathbf{H}}{\partial \mathbf{X}(0)}\right|_{\left(\mathbf{X}^{k}(0), \tau_r\right)} \Delta\mathbf{X} = \mathbf{0}, \tag{24}$$

then

$$\mathbf{J}^{SH}\left(\mathbf{X}^{k}(0), \tau_r\right)\Delta\mathbf{X} = -\mathbf{H}\left(\mathbf{X}^{k}(0), \tau_r\right), \tag{25}$$

where $\Delta\mathbf{X} = \mathbf{X}^{k+1}(0) - \mathbf{X}^{k}(0)$ represents the iterative increment of the state-space vector and $k$ is the Newton-Raphson iteration. The Jacobian matrix $\mathbf{J}^{SH}$ is a function of the state-space vector **X**(0) at iteration $k$ and defined by

$$\mathbf{J}^{SH}\left(\mathbf{X}^{k}(0), \tau_r\right) = \left.\frac{\partial \mathbf{H}}{\partial \mathbf{X}(0)}\right|_{\left(\mathbf{X}^{k}(0), \tau_r\right)} = \left.\frac{\partial \mathbf{X}}{\partial \mathbf{X}(0)}\right|_{\left(\mathbf{X}^{k}(0), \tau_r\right)} - \mathbf{I}, \tag{26}$$

with

$$\left.\frac{\partial \mathbf{X}}{\partial \mathbf{X}(0)}\right|_{\left(\mathbf{X}^{k}(0), \tau_r\right)} = \boldsymbol{\varphi}(\tau_r) = \begin{bmatrix} \boldsymbol{\Phi}(\tau_r) \\ \dot{\boldsymbol{\Phi}}(\tau_r) \end{bmatrix}, \tag{27}$$

where $\boldsymbol{\varphi}(\tau_r)$ is the monodromy matrix. The differentiation of Eq. (5) with respect to the vector **X**(0) yields

$$\mathbf{M}(t)\ddot{\boldsymbol{\Phi}} + \left(\mathbf{C}(t) + \frac{\partial \mathbf{F}_{be}}{\partial \dot{\boldsymbol{\delta}}}\right)\dot{\boldsymbol{\Phi}} + \left(\mathbf{K}(t) + \frac{\partial \mathbf{F}_{be}}{\partial \boldsymbol{\delta}}\right)\boldsymbol{\Phi} = \mathbf{0}. \tag{28}$$

Equation (28) is a system of linear differential equations. In order to solve it and to obtain the matrices $\boldsymbol{\Phi}(\tau_r)$ and $\dot{\boldsymbol{\Phi}}(\tau_r)$ forming the monodromy matrix $\boldsymbol{\varphi}(\tau_r)$, the linear version of the Newmark algorithm is used over one period $\tau_r$ of the rotor response.

The shooting algorithm solving simultaneously Eqs. (5) and (22) is presented as pseudo-code hereafter.

(1) Approached initial solution ${}^1\mathbf{X}(0)$

(2) Calculation of the state-space vector **X**

(3) Residual calculation **H** with Eq. (22)

(4) Calculation of the Jacobian matrix $\mathbf{J}^{SH}$ with Eq. (26)

(5) Newton-Raphson increment $\Delta\mathbf{X}$ with Eq. (25)

(6) Correction step $\mathbf{X}^{k+1}(0) = \mathbf{X}^{k}(0) + \Delta\mathbf{X}$

(7) If iterations $> I^{SH}$, increase the period of the rotor response and return to (1)

(8) If $\|\mathbf{H}\|/\|\mathbf{X}\| > \varepsilon^{SH}$, return to (2) for a new Newton-Raphson iteration, else stop the algorithm

After the periodic solution is obtained, its stability can be verified by applying the Floquet theory, i.e., by calculating the eigenvalues of the monodromy matrix called "Floquet multipliers". The solution is asymptotically stable if every Floquet multiplier remains inside a unit circle in the complex plane. When any Floquet multiplier leaves the unit circle, the periodic solution losses its stability and a bifurcation begins to appear. In practice, the saddle-node or period-doubling bifurcations occur if any Floquet multiplier leaves through +1 or through −1 respectively, while the quasi-periodic bifurcation occurs if two complex conjugate Floquet multipliers leave transversely the unit circle.

## 7 NUMERICAL RESULTS AND DISCUSSION

### 7.1 Configuration and Data

The symmetric rotor-hydrodynamic bearing system illustrated in Fig. 2 is excited by both a rotating mass unbalance and a sinusoidal translation of the base along the *Oz* axis expressed as $z_O=Z_O\cos(\Omega^z t)$ in m.

The physical properties as well as the geometry of the rotor and the bearings are listed in Table 1. The shaft is discretized with eight identical 2-node Timoshenko beam finite elements i.e., the total number of degrees of freedom is $n_g$=36. The disk is located at node 5 and the bearings # 1 and # 2 are placed at nodes 1 and 9 respectively, i.e., the corresponding localized non-linear degrees of freedom are 1-4 and 33-36. The rotor runs at a speed of rotation Ω=1200 rpm (=20 Hz, the mass unbalance frequency), the mass unbalance being located on the disk.

The relative coordinates of the static equilibrium position of the shaft geometric center in the fluid film bearings are given by $\boldsymbol{\delta}_{be}^{0}/c_{be}=<-0.29,-0.88>_R^T$.

The overall dynamic analysis of the non-linear on-board rotor is done by means of bifurcation diagrams, rotor orbits and Poincaré maps.

### 7.2 Bifurcation Diagrams

In the case of a harmonic external excitation of period $\tau_{ex}$, a linear rotor system has always a harmonic response of same period, i.e., $\tau_r=\tau_{ex}$, while a non-linear rotor system can have a non-periodic response or a periodic response with different period due to bifurcations. Such changes in the non-linear dynamic regime of the system can be identified by means of bifurcation diagrams.

Figure 3 shows the bifurcation diagram of the on-board rotor at the bearing # 2 (node 9) excited by the mass unbalance ($m_{mu}r_{mu}$=1500 g mm) and the sinusoidal translational motion of the base of frequency $\Omega^z$=80 Hz.

In the diagram, the amplitude $Z_O$ of the base motion is used as a bifurcation parameter to provide essential information about the Poincaré sections. The step used for this parameter $Z_O$ is $0.05\times10^{-5}$ m. Since the excitations due to the mass unbalance and to the base motions are sinusoidal and commensurable,

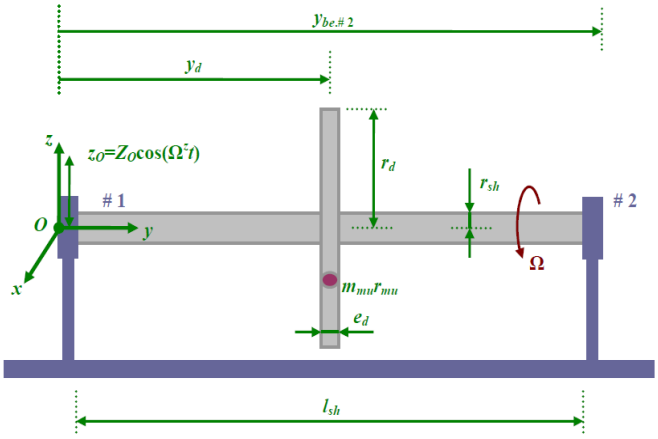


**Figure 2. ON-BOARD ROTOR-HYDRODYNAMIC BEARING SYSTEM CONFIGURATION**

**Table 1. ROTOR AND BEARING DATA**

| | |
|---|---|
| Disk material density | $\rho_d$=7800 kg/m$^3$ |
| Disk radius | $r_d$=0.15 m |
| Disk thickness | $e_d$=0.03 m |
| Disk location | $y_d$=0.2 m |
| Shaft material density | $\rho_{sh}$=7800 kg/m$^3$ |
| Young's modulus of the shaft | $E_{sh}=2\times10^{11}$ N/m$^2$ |
| Poisson's ratio of the shaft | $\nu_{sh}$=0.3 |
| Shaft radius | $r_{sh}$=0.04 m |
| Shaft length | $l_{sh}$=0.4 m |
| Mass unbalance | $m_{mu}r_{mu}$=1500 g mm, $\eta_{mu}$=0° |
| Radius of the bearings | $r_{be}$=0.04 m |
| Length of the bearings | $l_{be}$=0.01 m |
| Locations of the bearings | $y_{be.\#1}$=0 m, $y_{be.\#2}$=0.4 m |
| Radial clearance of the bearings | $c_{be}=2\times10^{-4}$ m |
| Oil film dynamic viscosity | $\mu_{be}=288\times10^{-4}$ Pa s |

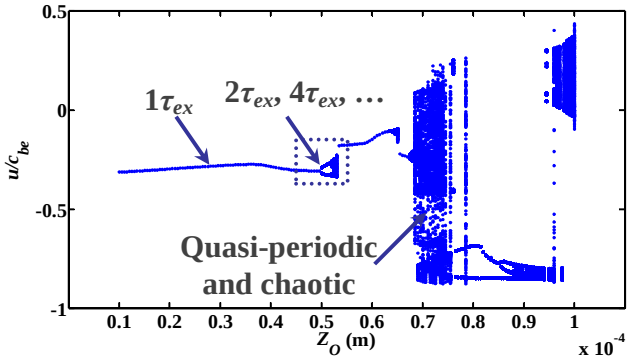


**Figure 3. BIFURCATION DIAGRAM OF THE ROTOR AT THE BEARING # 2 FOR A SINUSOIDAL TRANSLATION OF THE BASE: $z_O=Z_O\cos\Omega^z t$ WITH $\Omega^z$=80 Hz**

the external excitation of the rotor is harmonic of period $\tau_{ex}$ equal to the inverse of the greatest common factor of the mass unbalance frequency Ω=20 Hz and the base motion frequency $\Omega^z$=80 Hz. Thus the period of the external excitation of the

rotor is $\tau_{ex}$=1/20=0.05 s. The shooting algorithm is first run with $\tau_r=\tau_{ex}$, then with $\tau_r=2\tau_{ex}$, $\tau_r=3\tau_{ex}$, ... consecutively and limited with $\tau_r=16\tau_{ex}$. If the shooting method fails in finding a periodic solution, then the algorithm switches to a full transient time integration method which enables the computation of quasi-periodic and chaotic motions. The combination of the shooting method and the full transient time integration permits to speed up significantly the computation of the bifurcation diagram. The transient numerical simulations are executed with 1000 rotor revolutions (i.e., $1000\tau_{ex}$) and 512 time steps per period $\tau_{ex}$. The data of the first 500 revolutions of the rotor are not used in the bifurcation diagram in order to overcome the transient regime. The Poincaré sections are produced by considering successive intersections of the $x$ coordinates of the lateral dynamic motions of the rotor with the instants associated with the multiples of the period $\tau_{ex}$, i.e., $t=k\tau_{ex}$ and $k \in [501;1000]$. The initial conditions for the simulations are set to $\boldsymbol{\delta}_{be}{}^{0}/c_{be}$.

For $1\times10^{-5}\le Z_O\le4.95\times10^{-5}$ m, the rotor motion is harmonic of period $\tau_r=\tau_{ex}$ because there is only one point obtained by the Poincaré sections. Then, the first bifurcation appears and the rotor vibration displays a period-doubling orbit with $\tau_r=2\tau_{ex}$ when $5\times10^{-5}\le Z_O\le5.1\times10^{-5}$ m. At $Z_O$ =$5.15\times10^{-5}$ m, the rotor follows a quasi-periodic orbit, but it returns to the harmonic motion for $5.35\times10^{-5}\le Z_O\le6.3\times10^{-5}$ m. For the rest of the diagram, the solution of the equations of motion undergoes a series of bifurcations as shown in Fig. 3.

In order to visualize successive period-doubling bifurcations which lead to quasi-periodic responses and to chaos, a zoom of the bifurcation diagram is reproduced in Fig. 4 for the zone of interest $Z_O \in [4.5\times10^{-5};5.5\times10^{-5}\ \text{m}]$. This time, the step of the bifurcation parameter $Z_O$ is $0.01\times10^{-5}$ m. The finer grid allows a better observation of the changes of non-linear dynamic regime when compared with Fig. 3 for the same zone of interest. For example, the rotor motion holds $4\tau_{ex}$-periodic and $5\tau_{ex}$-periodic orbits (sub-harmonic) for $Z_O$ =$5.17\times10^{-5}$ m and $5.26\times10^{-5}$ m respectively.

The stability of some periodic solutions obtained in Fig. 4 is predicted using the Floquet theory. The monodromy matrix is calculated at the end of one period $\tau_r$ of the rotor response and its corresponding Floquet multipliers are presented in Fig. 5 within a unit circle in the complex plane. As can be seen, the solution is stable at the point *A* of Fig. 4 where $Z_O$=$4.95\times10^{-5}$ m with $\tau_r=\tau_{ex}$ (see Fig. 5(a)) and also at *C* where $Z_O$=$5\times10^{-5}$ m with $\tau_r=2\tau_{ex}$ (see Fig. 5(c)), while it is unstable and a period-doubling bifurcation occurs at *B* where $Z_O$=$4.96\times10^{-5}$ m with $\tau_r=\tau_{ex}$ (see Fig. 5(b)) because one of the Floquet multipliers leaves the circle through the negative real axis at −1. This can be verified with the orbit of the rotor at the bearing # 2 which is $1\tau_{ex}$-periodic (see Fig. 6(a)) for the point *A* and becomes $2\tau_{ex}$-periodic (see Fig. 6(b)) for the point *C*.

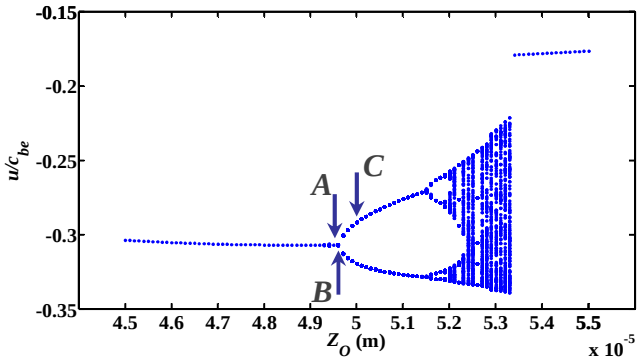


**Figure 4. ZOOM ON THE BIFURCATION DIAGRAM IN FIG. 3 FOR THE ZONE OF INTEREST $Z_O \in [4.5\times10^{-5};5.5\times10^{-5}\ \text{m}]$**

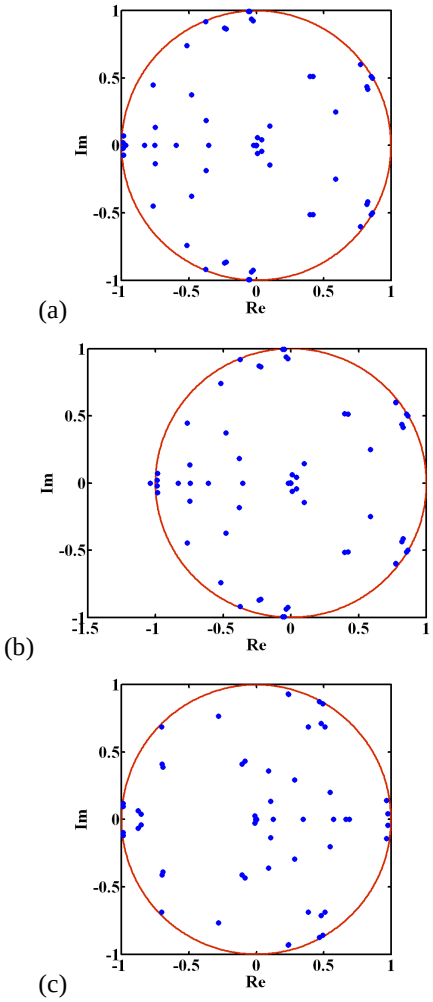


**Figure 5. EIGENVALUES OF THE MONODROMY MATRIX CORRESPONDING TO THE POINTS *A*,*B* AND *C* IN FIG. 4 ASSOCIATED WITH: $Z_O$= (a) $4.95\times10^{-5}$ m, (b) $4.96\times10^{-5}$ m, (c) $5\times10^{-5}$ m, RESPECTIVELY**

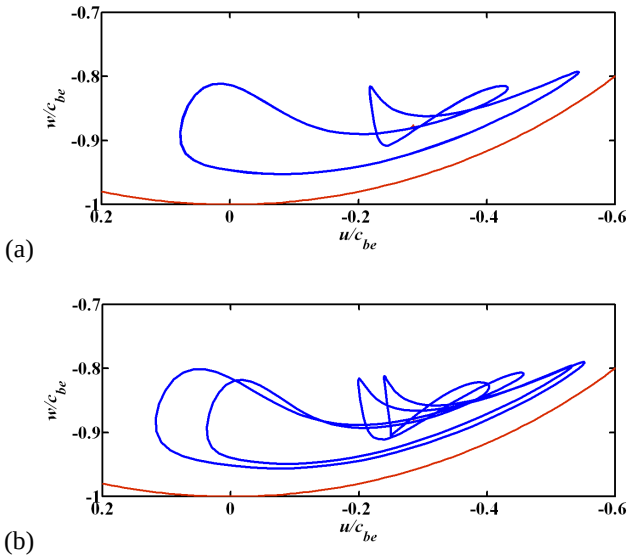


**Figure 6. ORBITS OF THE ROTOR AT THE BEARING # 2 OBTAINED WITH THE SHOOTING METHOD FOR THE POINTS (a) *A*, AND (b) *C* OF FIG. 4**

### 7.3 Bifurcation Responses of the Rotor-Bearing System

In this section, some orbits of the rotor and their projected Poincaré maps at the bearing # 2 (node 9) corresponding to values of interest of the bifurcation parameter $Z_O$ of the bifurcation diagram in Fig. 3 are presented.

All the orbits are made dimensionless with respect to the bearing clearance $c_{be}$ and are thus plotted within a unit circle (red curve).

The relative coordinates of the static equilibrium position of the shaft center in the bearings $\boldsymbol{\delta}_{be}{}^{0}/c_{be}$ are used as initial conditions for the transient dynamic calculations. The Poincaré maps are obtained by taking successive intersections of the relative dynamic displacements of the rotor with the instants corresponding to the multiples of the period $\tau_{ex}$=0.05 s of the harmonic external excitation of the rotor starting from $t$=501$\tau_{ex}$ to eliminate the transient effects.

When the amplitudes $Z_O$ of the base translation are consecutively equal to $7\times10^{-5}$ m (Fig. 7(a)), $9\times10^{-5}$ m (Fig. 7(b)) and $9.45\times10^{-5}$ m (Fig. 7(c)), the rotor displacements exhibit a chaotic orbit, a quasi-periodic orbit and a sub-harmonic orbit ($8\tau_{ex}$-periodic) respectively.

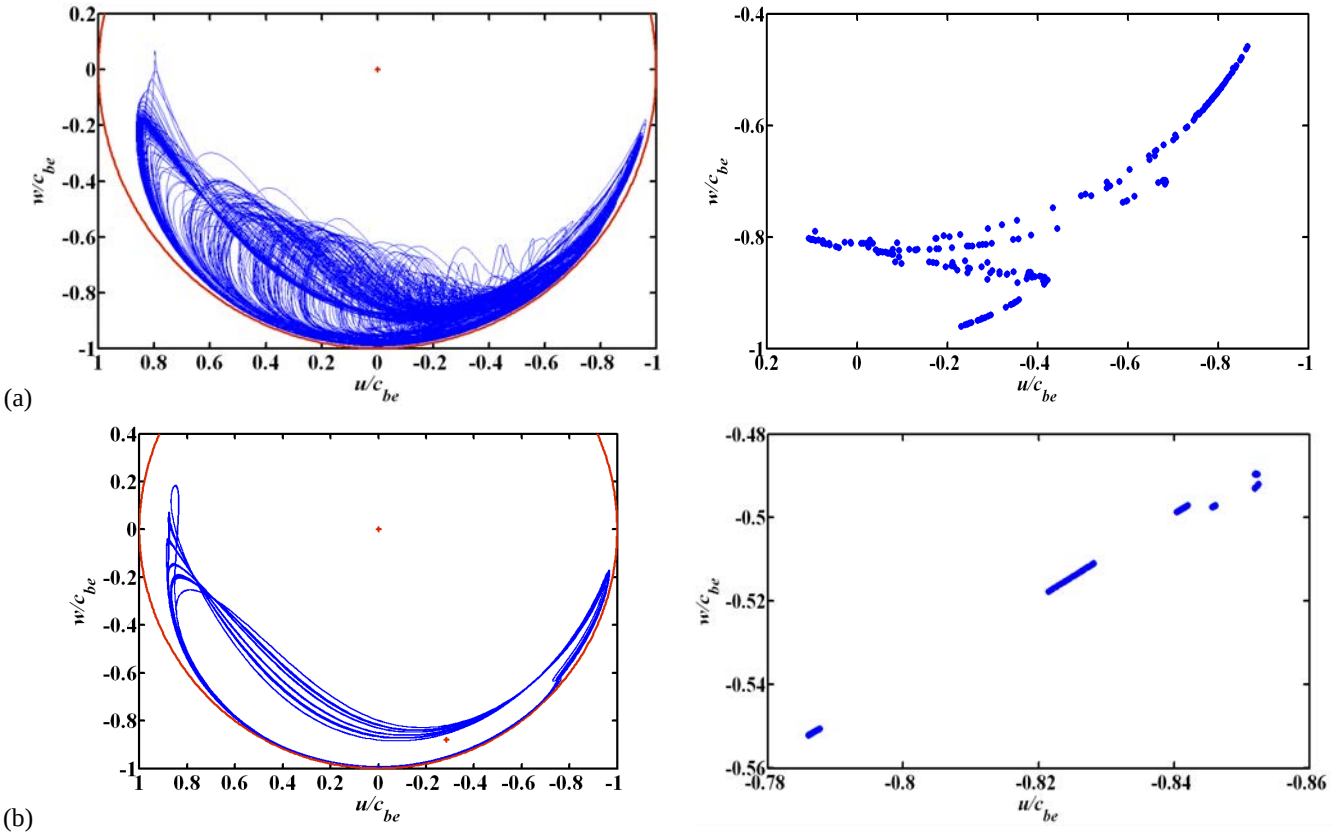

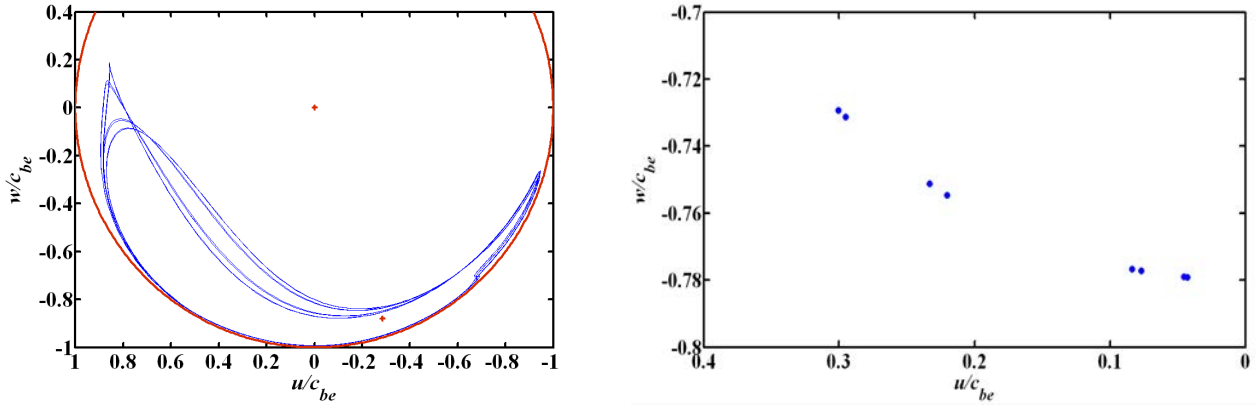


(c)

**Figure 7. ORBITS AND POINCARÉ MAPS OF THE ROTOR AT THE BEARING # 2 DUE TO SINUSOIDAL TRANSLATIONS OF THE BASE: $z_O=Z_O\cos\Omega^z t$ WITH $\Omega^z$=80 Hz AND $Z_O$= (a) 7×10$^{-5}$ m, (b) 9×10$^{-5}$ m, (c) 9.45×10$^{-5}$ m**

## 8 CONCLUDING REMARKS

A finite element model based on the Timoshenko beam theory is presented to analyze the dynamic behavior of a symmetric on-board rotor-non-linear hydrodynamic bearing system whose base is subject to sinusoidal translations.

The derivation of the equations of motion shows that the base rotations create time-varying parametric coefficients, while the base translations contribute only to the external force vector.

Robust Newmark integration and shooting algorithms combined with the Newton-Raphson iterative procedure are used to obtain the dynamic responses of the on-board rotor.

It is noted that depending on the amplitudes of the sinusoidal motions of the base, non-linear phenomena, such as period-doubling and quasi-periodic motions and transition to chaos, are observed by means of bifurcation diagrams and rotor responses. The stability of periodic solutions is verified using the Floquet theory.

## REFERENCES


[1] Lalanne, M., and Ferraris, G., 1998, *Rotordynamics Prediction in Engineering*, Wiley, Chichester.

[2] Genta, G., 2005, *Dynamics of Rotating Systems*, Springer, New York.

[3] Berlioz, A., Dufour, R., and Sinha, S. C., 2000, "Bifurcation in a Nonlinear Autoparametric System Using Experimental and Numerical Investigations," Nonlinear Dyn., **23**(2), pp. 175-187.

[4] Oncescu, F., Lakis, A. A., and Ostiguy, G., 2001, "Investigation of the Stability and Steady State Response of Asymmetric Rotors, Using Finite Element Formulation," J. Sound Vib., **245**(2), pp. 303-328.

[5] Li, D., and Xu, J., 2004, "A Method to Determine the Periodic Solution of the Non-linear Dynamics System," J. Sound Vib., **275**(1-2), pp. 1-16.

[6] Chen, C.-K., and Yau, H.-T., 2001, "Bifurcation in a Flexible Rotor Supported by Short Journal Bearings With Nonlinear Suspension," J. Vib. Control, **7**(5), pp. 653-673.

[7] Shi, M., Wang, D., and Zhang, J., 2013, "Nonlinear Dynamic Analysis of a Vertical Rotor-Bearing System," J. Mech. Sci. Technol., **27**(1), pp. 9-19.

[8] Srinivasan, V., and Soni, A. H., 1984, "Seismic Analysis of a Rotor-Bearing System," Earthq. Eng. Struct. Dyn., **12**(3), pp. 287-311.

[9] Hori, Y., and Kato, T., 1990, "Earthquake-Induced Instability of a Rotor Supported by Oil Film Bearings," ASME J. Vibr. Acoust., **112**(2), pp. 160-165.

[10] Kang, Y., Chang, Y.-P., Tsai, J.-W., Mu, L.-H., and Chang, Y.-F., 2000, "An Investigation in Stiffness Effects on Dynamics of Rotor-Bearing-Foundation Systems," J. Sound Vib., **231**(2), pp. 343-374.

[11] Cavalca, K. L., Cavalcante, P. F., and Okabe, E. P., 2005, "An Investigation on the Influence of the Supporting Structure on the Dynamics of the Rotor System," Mech. Syst. Signal Proc., **19**(1), pp. 157-174.

[12] Duchemin, M., Berlioz, A., and Ferraris, G., 2006, "Dynamic Behavior and Stability of a Rotor Under Base Excitation," ASME J. Vibr. Acoust., **128**(5), pp. 576-585.

[13] Driot, N., Lamarque, C. H., and Berlioz, A., 2006, "Theoretical and Experimental Analysis of a Base-Excited Rotor," ASME J. Comput. Nonlinear Dyn., **1**(3), pp. 257-263.

[14] El-Saeidy, F. M. A., and Sticher, F., 2010, "Dynamics of a Rigid Rotor Linear/Nonlinear Bearings System Subject to Rotating Unbalance and Base Excitations," J. Vib. Control, **16**(3), pp. 403-438.

[15] Das, A. S., Dutt, J. K., and Ray, K., 2010, "Active Vibration Control of Unbalanced Flexible Rotor-Shaft Systems Parametrically Excited Due to Base Motion," Appl. Math. Model., **34**(9), pp. 2353-2369.

[16] Dakel, M., Baguet, S., and Dufour R., 2012, "Investigation on the Dynamics of an On-Board Rotor-Bearing System," Proceedings of the ASME 2012 International Design Engineering Technical Conferences & Computers and Information in Engineering Conference, Chicago, Illinois, USA, Aug. 12-15.

[17] Dakel, M., Baguet, S., and Dufour R., "Steady-State Dynamic Behavior of an On-Board Rotor Under Combined Base Motions," J. Vib. Control, http://dx.doi.org/10.1177/1077546313483791. (in press).

[18] Dakel, M., Baguet, S., and Dufour R., 2014, "Nonlinear Dynamics of a Support-Excited Flexible Rotor With Hydrodynamic Journal Bearings," J. Sound Vib., **333**(10), pp. 2774-2799.

[19] Frêne, J., Nicolas, D., Degueurce, B., Berthe, D., and Godet, M., 1997, *Hydrodynamic Lubrication Bearings and Thrust Bearings*, Elsevier Science, Amsterdam.